Journal of Renewable Materials
DOI:10.32604/jrm.2020.010991
Article

Tech Science Press

Mechanical Properties of Sea Water Sea Sand Coral Concrete Modified with Different Cement and Fiber Types

Xibo Qi[1], Yijie Huang[2,3,*], Xiaowei Li[1], Zhenhua Hu[1], Jingwei Ying[3] and Dayong Li[1]

[1]Department of Building Engineering, Shandong University of Science & Technology, Qingdao, 266590, China
[2]Shandong Key Laboratory of Civil Engineering Disaster Prevention and Mitigation, Shandong University of Science and Technology, Qingdao, 266590, China
[3]Guangxi Key Laboratory of Disaster Prevention and Engineering Safety, Guangxi University, Nanning, 530004, China
*Corresponding Author: Yijie Huang. Email: 302huangyijie@163.com
Received: 13 April 2020; Accepted: 27 May 2020

Abstract: The mechanical properties of modified sea water sea sand coral concrete (SWSSCC) under axial compression were experimentally studied. Two different parameters were considered in this test: types of cement and fiber. An experimental campaign was developed involving uniaxial compression tests and the use of digital image correlation (DIC) method to analyze the strain distribution and crack propagation of specimen. Test results indicated that the compressive strength and elastic modulus of SWSSCC were improved by adding stainless steel fibers (SSF), while polypropylene fibers (PF) enhanced the SWSSCC peak deformation. It was found that the elastic modulus and strength of SWSSCC using ordinary Portland cement (OPC) were higher compared to specimen with low alkalinity sulphoaluminate cement (LAS). Typical strain distribution changed with the variation of fiber types. The propagation and characteristics of cracks in SWSSCC containing PF were similar to those of cracks in SWSSCC. However, the propagation of cracks and the development of plastic deformation in SWSSCC were effectively hindered by adopting SSF. Finally, an analytical stress-strain expression of specimen considering the influences of fibers was established. The obtained results would provide a basis for the application of SWSSCC.

Keywords: Sea water sea sand coral concrete; modified concrete; mechanical properties; stress-strain curve; crack propagation; strain distribution

Notation

a, b:	parameters in stress-strain curve
d_{sf}:	diameter of SSF
d_{pf}:	diameter of polypropylene fibers (PF)
E_c:	elastic modulus of concrete
f_a:	tube compressive strength of coral coarse aggregates
f_c:	prismatic compressive strength of concrete
f_{cu}:	cubic compressive strength of concrete
$f_{cu,k}$:	standard value of concrete cubic compressive strength

l_{sf}: length of SSF
l_{pf}: length of PF
Q_a: clay dosage of aggregates
W: water absorption of aggregates
α: Cl^- content in cement mortar
β: shell content in sea sand
ε_c: peak strain of concrete
ε: axial strain of concrete
υ_o: initial Poisson's ratio
υ: Poisson's ratio
λ_{sf}: characteristic value of SSF
λ_{pf}: characteristic value of PF
ρ_o: apparent density of aggregates
ρ_{sf}: volume fraction of SSF
ρ_{pf}: volume fraction of PF
σ_c: axial stress of concrete
σ_{max}: peak stress of sliced concrete

1 Introduction

The construction of islands in the ocean has become a new imperative for China due to the implementation of marine development strategy in recent years. However, these islands are far away from the mainland and lack fresh water, river sand and gravel, which need ships to transport construction materials [1]. The construction cost is increased and the period is extended. Therefore, finding an alternative concrete made from environmentally-friendly materials becomes important.

Sea water sea sand coral concrete (SWSSCC) can replace fresh water, river sand and gravel with sea water, sea sand and coral coarse aggregate (CCA), respectively. Sea water, sea sand and coral aggregate have many advantages such as locally available materials and low cost [2]. The application of SWSSCC saves the terrestrial resources and makes full use of the ocean resources. SWSSCC is an important environmentally friendly material. However, sea water and sea sand contain many chloride ions (Cl^-), sulfates (SO_4^{2-}) and shell particles [3], and coral coarse aggregates contain many holes. The mechanical properties of SWSSCC are complicated. Typical influences of sea water, sea sand and coral aggregate on the properties of concrete have been studied in recent years. The physical properties varied with the variation of material composition. It was shown that sea water affected the setting time of concrete, and the workability of sea water concrete (SWC) was improved by adding the appropriate admixture [4,5]. The microstructure and hydration products of SWC were different from those of ordinary concrete (concrete using gravels/pebbles, river sand and fresh water) [6]. It was found that axial compressive strength of SWC was higher than that of ordinary concrete at early age [7–9], while these differences were negligible after long-term exposure [10,11]. The corrosion of reinforced SWC was serious due to the influences of Cl^- and SO_4^{2-}, while the corrosion can be reduced by adding the mineral admixture such as metakaolin [12–14]. Etxeberria et al. [9] reported that the plastic shrinkage of SWC was low compared to ordinary concrete. Typical influences of sea sand on workability, mechanical properties and durability were similar to those of sea water due to the addition of Cl^- [15–17]. But sea sand reduced the fluidity and strength of concrete due to shell particles.

There have been several experimental studies on the mechanical properties of coral aggregate concrete (CAC). Arumugam et al. [18], Wang [19] and Ehlert [20] found that strength of coral aggregate concrete was higher than that of ordinary concrete at early age. The 7d compressive strength of CAC was about 85–90% of

28 d compressive strength, and the growth of CAC strength was likely to slow down after 7 d. It was verified that CAC exhibited a 56% increase in strength after 11 years [20]. The workability of CAC was accepted after adding additional water [21]. It was found that axial compressive strength of CAC increased with a decrease in water-cement ratio [2,21]. Furthermore, adding fibers (carbon fiber and sisal fiber, etc.) and mineral admixtures (metakaolin and silica fume) would enhance the strength of CAC [22,23].

These above studies provided references for the application of the SWSSCC. But the current studies mainly focused on basic mechanical properties of SWSSC. The load-deformation relationship and deformability were not systematically studied. Wang et al. [24] and Da et al. [2] obtained the whole stress-strain curve of sea water coral concrete. It was found that the ascent stage of sea water coral concrete was similar to that of ordinary concrete, while the failure of sea water coral concrete was brittle. The ductility of coral aggregate concrete was low compared to ordinary concrete. The application of SWSSCC is restricted due to the above shortcomings.

At present, there are few studies on the improvement of the strength and ductility of SWSSCC. In this test, different types of cement (OPC, LAS) and fibers were considered to enhance the properties of SWSSCC, which was attributed to LAS cement and fibers (SSF, etc.) could not only reduce the negative influence of sulfates but also improve the mechanical properties and durability. An experimental system was developed involving a uniaxial compression test and the use of digital image correlation (DIC) method. It can obtain the mechanical properties of SWSSCC and analyze the strain distribution and crack propagation of specimen. The study provided deeper insight into the elastic development, cracking and failure of modified SWSSCC. The variations in mechanical properties of concrete at macro-and micro-scales were investigated. Finally, an analytical stress-strain expression was also proposed. The obtained results would provide a basis for the practical application of modified SWSSCC.

2 Experimental Program

2.1 Materials

42.5R ordinary Portland cement (OPC) and low alkalinity sulphoaluminate cement (LAS) were adopted. Typical characteristics of LAS can be described as high frost and corrosion resistances and good impermeability [25]. The X-ray fluorescence analysis method was used to obtain the chemical composition of cement (Tab. 1). The fine and coarse aggregates were sea sand and coral coarse aggregate (CCA), respectively (Fig. 1). Detailed particle size distribution of aggregates is shown in Fig. 2. The mixing water was sea water which was obtained from Qingdao harbor of China. The main ions in seawater were obtained by the ion chromatography method. Basic properties/composition of aggregates and water are listed in Tabs. 2 and 3.

The mix proportion in the test was Cement: Sand: Coarse aggregate: Water = 1: 1.3: 2.6: 0.43. The mix proportion of specimen was designed according to the related standard [26]. The target strength of specimen was about C30-C35, which was commonly used in the world.

Furthermore, stainless steel fibers (SSF) and polypropylene fibers (PF) were used in this test (Fig. 3). The diameter and length of SSF (PF) were 1.42 mm (0.048 mm) and 37 mm (18 mm), respectively. The strength, elastic modulus and density of SSF (PF) were 360 MPa (412 MPa), 2.1×10^5 MPa (4×10^3 MPa) and 7.8 g/cm^3 (0.91 g/cm^3), respectively.

2.2 Specimen Details and Testing Instruments

The concrete mixes were prepared as follows. Firstly, cement, sea sand and 1/3 of sea water were added and mixed for about 2 min. Secondly, coral coarse aggregates and 1/3 of sea water were added and mixed for 2 min. Finally, adding fibers and the remaining sea water, and mixing it uniformly. All specimens were immersed in sea water until the test age of 28 days (temperature: 20 ± 2°C).

Table 1: Chemical composition of cements

	Al_2O_3 (%)	SiO_2 (%)	Fe_2O_3 (%)	CaO (%)	SO_2 (%)	R_2O (%)	MgO (%)	Others (%)	Loss on ignition (%)
OPC	6.02	21.82	3.65	60.79	2.21	0.59	2.07	0.72	2.13
LAS	30.55	10.65	2.49	42.44	9.27	0.35	2.52	0.71	1.02

(a) (b)

Figure 1: Coarse and fine aggregates (a) Coral coarse aggregates (b) Sea sand

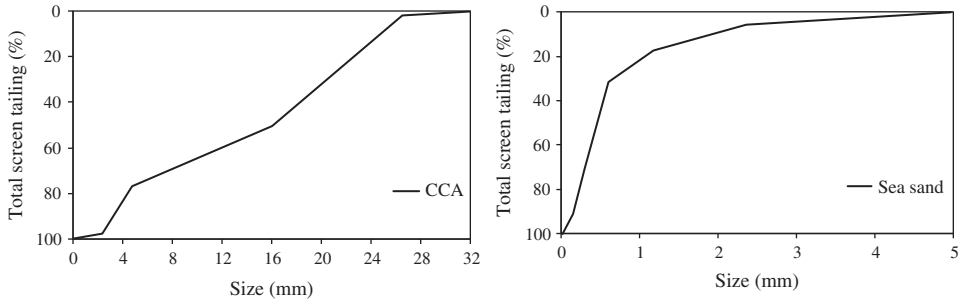

(a) (b)

Figure 2: Particle size distribution (a) Fine aggregates (b) Coarse aggregates

Table 2: Basic properties of coarse aggregates

	Size (mm)	Bulk density (kg/m^3)	Apparent density (kg/m^3)	Water absorption (%)	Clay dosage (%)	Shell content (%)
CCA	5–25	978	1850	12.9	8.6	–
Sea sand	0.15–4.75	1620	2635	–	0.8	1.8

* Bulk density is obtained under the dry condition.

Table 3: The main ions of sea water

Ingredients	Cl^-(μg/l)	Na^+(μg/l)	SO_4^{2-}(μg/l)	Mg^{2+}(μg/l)	Ca^+(μg/l)
	19831	16563	1936	777	888

(a) (b)

Figure 3: Stainless steel fiber and polypropylene fiber (a) Stainless steel fibers (b) Polypropylene fibers

There were 7 different groups of SWSSCC considering the types of cement and fiber. Each group had 54 prismatic specimens (100 × 100 × 300 mm^3) and 54 cubic specimens (100 × 100 × 100 mm^3). Furthermore, there were 3 sliced specimens (100 × 100 × 15 mm^3) in each group to study the crack propagation and strain distribution of specimen. The sliced specimen was cut from cubic concrete by a rock cutter.

Specimen was named according to test parameters (Tab. 4). PC and SC represent SWSSCC adopting OPC and LAS, respectively. SC-P and SC-S denote SC using PF and SSF, respectively. SC-PS represents SC adopting both PF and SSF. Taking "SC-P-A" as an example, "SC-P" denotes SWSSCC adopting low alkalinity sulphoaluminate cement and polypropylene fiber, "A" represents the fiber addition is 1.0 kg/m^3. Details of specimen are listed in Tab. 4.

Table 4: Details of specimen

No.	Specimen	Type of cement	SSF (%)	PF (kg/m^3)	Cl^- in cement mortar (%)	Characteristic values of SSF	Characteristic values of PF
1	PC	OPC	–	–	0.40	–	–
2	SC	LAS	–	–	0.33	–	–
3	SC-S-A	LAS	1.0	–	0.33	0.26	–
4	SC-S-B	LAS	1.5	–	0.33	0.39	–
5	SC-P-A	LAS	–	1.0	0.33	–	0.75
6	SC-P-B	LAS	–	1.5	0.33	–	1.10
7	SC-PS	LAS	1.47	1.21	0.33	0.38	0.89

*The percentage for added stainless steel fiber is by volume. The volume fractions of SC-P-A and SC-P-B were 0.11% and 0.16%, respectively. The volume fraction of PF in SC-PS was 0.13%.

2.3 Test Instruments and Loading Program

Two different loading systems were adopted to obtain the mechanical properties of specimen. The loading systems for prismatic/cubic specimen and sliced specimen are shown in Figs. 4a and 4b, respectively.

The loading system for prismatic/cubic specimen consisted of two parts (Fig. 4a): a 2000 kN electro-hydraulic servo tester and a computer system. The recorded axial displacement was deformation of mid-span of prismatic concrete (100 mm). The loading system for sliced concrete (Fig. 4b) included an electro-hydraulic servo tester (400 kN), a video system with 1 million resolution industrial camera, and the lighting and computer systems. Two strain gauges were pasted on both sides of sliced concrete to measure axial deformation of specimen.

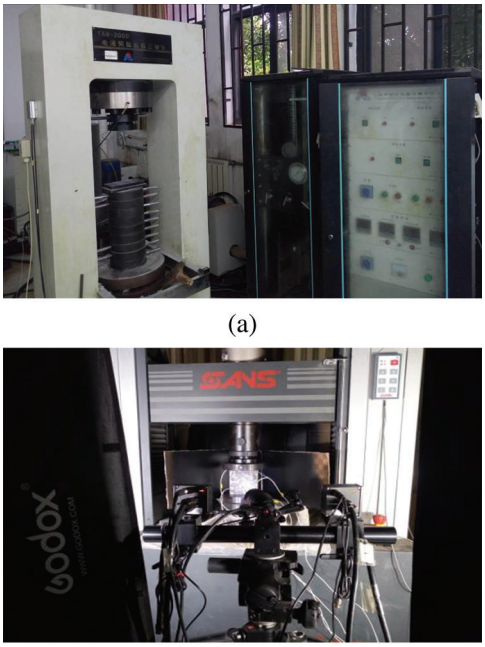

(a)

(b)

Figure 4: Loading systems (a) Prismatic and cubic specimens (b) Sliced concrete

2.4 Experimental Procedure

2.4.1 Prismatic and Cubic Specimens

The loading mode of experiment was in the form of displacement pattern, and the loading rate was 0.07 mm/min considering the efficiency and data. All specimens were preloaded with 10% of the predicted peak load before actual experiment to ensure normal work of test set-up. The deformation measurement system included strain gauges and displacement transducers. Axial and transverse deformations of prismatic specimens were measured with the linear displacement sensors (YHD-50) and the strain gauges. The deformation was recorded by data acquisition system (DH5902), and the period of data acquisition was 0.2 s.

2.4.2 Sliced Specimen

The loading mode and rate of sliced concrete were similar to those of prismatic concrete. The sliced specimen was preloaded with 2 kN before actual loading, which lessened the stress concentration and ensured normal work of loading devices. Two 100 mm strain gauges were pasted on both sides of specimen. The uniform axial deformation of sliced specimen was obtained by strain gauges. Test results were recorded by data acquisition system, and the period of data acquisition was 0.5 s. Axial strain gauges only obtained the ascent stage of stress-strain curve precisely due to the cracking of concrete. The displacement transducers installed in electro-hydraulic servo tester was used to measure the declining stage of curve.

Furthermore, a video system was utilized to obtain digital information of specimen. The period of image acquisition was 0.5 s.

3 Experimental Results and Discussion

3.1 Experimental Phenomena

3.1.1 Failure Process

Axial stress increased linearly with the increase in deformation at the initial stage of loading. The load-deformation curve of modified SWSSCC became nonlinear when axial stress was 30 % of the peak stress (f_c).

The visible fine crack was observed after axial stress reached 0.8–0.9 f_c, while its size was small. It was found that cracks increased rapidly when axial stress approached f_c. But cracks in SWSSCC with SSF propagated steadily and the brittle failure of specimen was not observed. This is because SSF prevent the development of macro-cracks. However, cracking of SWSSCC with PF developed quickly compared to SC-S-A and SC-S-B. This is due to the low elastic modulus of PF. Typical failure of SWSSCC with PF was brittle. Furthermore, the failure process of SWSSCC was not changed after mixing different concrete types. It was shown that cracks drastically propagated after f_c, and the SC and PC specimens failed suddenly. It can be attributed to the interlocking mechanism of PC and SC failed after f_c.

3.1.2 Failure Surface

Typical failure patterns of modified SWSSCC are shown in Fig. 5. It was found that inclination angle between macro-cracks and loading direction of PC was about 35°–40°, however, the inclination angle of SC was 30°–35°. The failure surface of SC was smooth and all coral coarse aggregates were broken compared to SC-S-A and SC-S-B (Fig. 6a). It was verified that the interlocking mechanism between cement mortar and coral coarse aggregates failed after f_c. Furthermore, the inclination angle of specimen with SSF (SC-S-A, SC-S-B) was about 25°–35° (Fig. 5). Typical failure surface of SC-S-B was smooth and most of coarse aggregates were broken (Fig. 6b), while steel fibers were seldom damaged. It was shown that steel fibers not only delayed propagation of crack but also provided interlocking action after the peak stress. Furthermore, typical failure surface of SWSSCC with PF is shown in Fig. 6c. Most of polypropylene fibers were broken. However, a few of fibers were intact. It was found that PF just delayed crack propagation. The interlocking action between CCA and cement was not improved (SC-P) after the peak stress. The failure of SWSSCC with PF was brittle.

3.2 Poisson's Ratio

3.2.1 Initial Poisson's Ratio

The initial Poisson's ratio (υ_o) of specimen is listed in Tab. 5. Details of experimental procedure could be found in [2]. It was found that υ_o increased with an increase in SSF content. Test results indicated that υ_o of SC-S-B was high compared to other specimens.

The υ_o changed with the variation of cement type. It was found that υ_o of PC (0.24) was 12.9% lower than that of PC. The υ_o of SC-P-A and SC-P-B were 0.7% and 3.7% lower than that of SC, respectively. Therefore, the statistical analysis (ANOVA method) was used to determine that, and Matlab software was adopted to code the related program. The PF effect on υ_o of SWSSCC was negligible according to ANOVA analysis. Furthermore, υ_o of specimen containing PF and SSF (SC-PS) was about 20.7% higher than that of SC.

3.2.2 Development of υ

The lateral deformation coefficient (υ) is the ratio of transverse strain to axial strain. Typical development of υ of modified SWSSCC is shown in Fig. 7. It was found that υ was small at the early stage of test. It became large (0.4–0.6) when axial stress (σ) reached 70%–90% of f_c due to micro-cracking of concrete. Test results indicated that υ drastically increased when stress approached f_c. It was found that υ of SC-S developed slowly compared to other specimens. This is because steel fibers delay the crack propagation and restrain the development of transverse deformation.

3.3 Elastic Modulus

The elastic modulus of specimen (E_c) is listed in Tab. 5 [2]. It was found that E_c increased with an increase in SSF content. The E_c of SC-S-B was about 5.6% higher than that of SC-S-A. This difference is attributed to the high modulus of steel fiber.

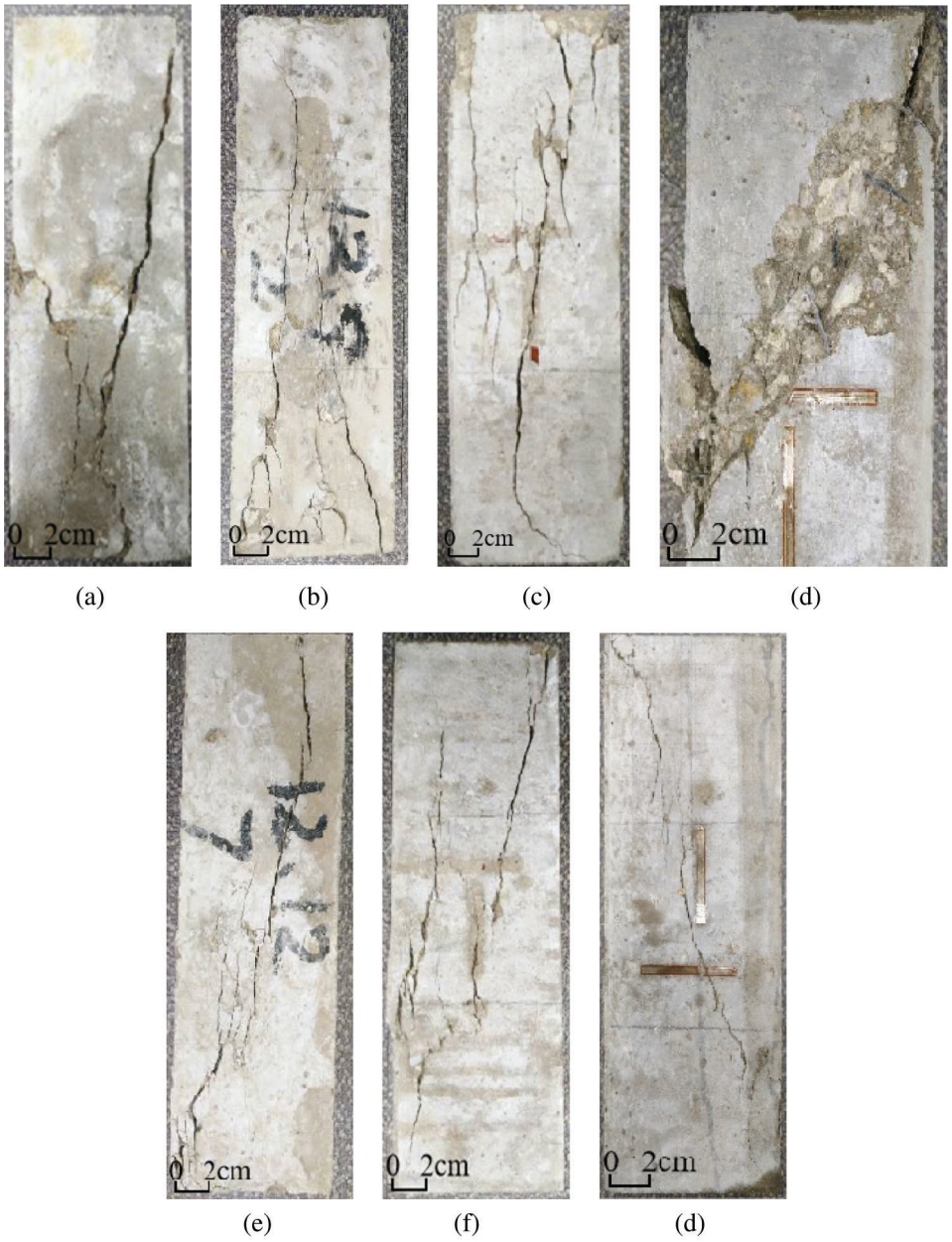

Figure 5: Typical failure of prismatic specimen (a) PC (b) SC (c) SC-S-A (d) SC-S-B (e) SC-P-A (f) SC-P-B (g) SC-PS

Furthermore, typical influence of PF on E_c varied with the variation of content. It indicated that E_c of SC-P-A was 1.42% lower than that of SC, while E_c of SC-P-B was 0.6% higher than that of SC. This is because the combined results of the low modulus of PF and the improvement of concrete properties by PF. The influence of PF on E_c was negligible by ANOVA analysis.

It was verified that E_c of specimen containing PF and SSF (SC-PS) was higher than that of SC due to high modulus of steel fiber. E_c changed with the variation of cement type. The elastic modulus of PC was 4.6% higher than that of SC. The influence of LAS on E_c of SWSSCC was improved by adding SSF compared to PF. It was found that E_c of SC-S-B was 2.3% higher than that of PC.

Figure 6: Failure surface (a) SC (b) SC-S-B (c) SC-P-B

Table 5: Experimental results

Group No.	Specimen	v_o	E_c ($\times 10^4$MPa)	f_c (MPa)	f_c/f_{cu}	ε_c (ε)
1	PC	0.240	2.57	37.8	0.86	0.002265
2	SC	0.271	2.46	34.4	0.93	0.002224
3	SC-S-A	0.267	2.49	34.2	0.92	0.002183
4	SC-S-B	0.349	2.63	38.8	0.98	0.002435
5	SC-P-A	0.269	2.42	31.2	0.90	0.002312
6	SC-P-B	0.261	2.47	36.3	0.98	0.002568
7	SC-PS	0.327	2.58	36	0.91	0.002474

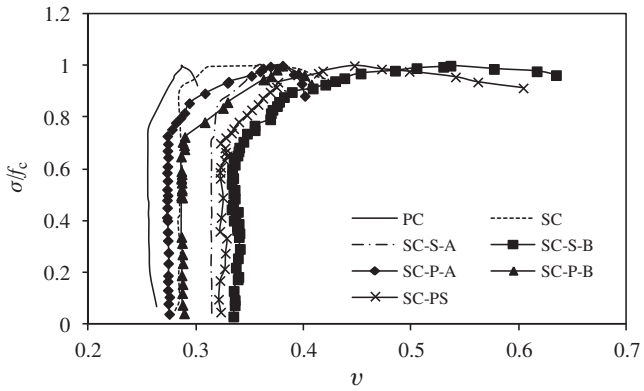

Figure 7: The development of lateral deformation coefficient

3.4 Compressive Strength

3.4.1 Prismatic Compressive Strength (f_c)

SSF enhanced prismatic compressive strength of SWSSCC (Fig. 7), and f_c increased with an increase in SSF content. The f_c of SC-S-B was about 13.4% and 12.9% higher than those of SC-S-A and SC, respectively. This is because steel fibers delay the development of cracks and improve the mechanical properties.

The compressive strength changed with the variation of PF content. It was found that f_c was decreased when PF content was less than a certain value. The f_c of SC-P-A was 5.6 % lower that of SC, while f_c of SC-P-B was 0.5 % higher than SC. It can be attributed to the combined effects of low modulus of PF and improvement of concrete properties by PF. Based on ANOVA analysis, the effect of PF on f_c became small when PF content was less than a certain value (1.0 kg/m^3). Furthermore, f_c was improved after mixing different types of fibers. The prismatic compressive strength of SC-PS was high compared to SC.

Test results indicated that f_c changed with the variation of cement type. The compressive strength of SWSSCC using OPC (PC) was about 9.9% more than that of SWSSCC adopting LAS (SC). The reasons for this phenomenon are as follows. (1) Sea water with high Cl^- concentration restrains SO_4^{2-} from binding with cement (tricalcium aluminate, C_3A) and significantly decreases the sulfates attack of concrete [27,28]. The negative influences of sulfates attack on micro-and macro-structures of concrete become negligible. (2) The C_3A content of OPC is high compared to LAS. The Cl^- (sea water and sea sand) react with C_3A to form Friedel's salt in concrete. Etxeberria et al. [5] observed that the porosity of sea water concrete was reduced and the compressive strength was improved due to an accumulation of salts in pores of concrete [29]. The more C_3A in cement is, the more Friedel's salt in SWSSCC is, and the higher strength is.

Furthermore, SSF reduced the effect of LAS on SWSSCC compressive strength. The f_c of SC-S-B was about 3 % more than that of PC.

3.4.2 f_c/f_{cu}

The ratio of prismatic compressive strength (f_c) to cubic compressive strength (f_{cu}) is listed in Tab. 5 (f_c/f_{cu}). Test results indicated that f_c/f_{cu} of modified SWSSCC (0.85) was higher than that of ordinary concrete [30]. The f_c/f_{cu} increased with the increases in PF and SSF contents. But the influence of OPC on f_c/f_{cu} was negative.

3.5 Peak Strain

The peak stain (ε_c) is the axial strain corresponding to f_c (Tab. 5). It was verified that ε_c increased with an increase in f_c. The polypropylene fibers obviously enhanced the peak strain of SWSSCC, while the influence of SSF on ε_c was small. Test results indicated that ε_c of specimen with PF (SC-P) was averagely 5.7 % higher than ε_c of specimen with SSF (SC-S). That can be explained as the polypropylene fibers decrease modulus of concrete, which leads to an increase in deformation.

The ε_c of SC was more than that of PC by adding SSF or PF. It was found that a 10 percent increase of ε_c was obtained for the SC-S-B and SC-P-B compared to PC.

3.6 Stress-Strain Curve

The stress-strain curve (SSC) of modified SWSSCC was divided into elastic, elastic-plastic ascending and declining stages (Fig. 8).

1. Elastic Stage

Axial stress increased linearly with an increase in strain in this stage (about 0.1–0.3f_c). The slope of PC curve was more than that of SC (Fig. 8a). It was found that SSF improved the slope of SSC (Fig. 8b). Furthermore, typical influence of PF on initial slope of SSC was positive when PF content was more than a certain value. The slope of SC-P-B curve was high compared to SC.

2. Elastic-Plastic Ascending Stage

The relationship between axial stress and strain was nonlinear in the elastic-plastic ascending stage (about 0.3–1.0 f_c). It was found that the curvature of SC stress-strain curve was higher than that of PC stress-strain curve (Fig. 8a). This is because the Friedel's salt in PC fills pores, improves physical properties of cement mortar [5] and decreases the plastic deformation and micro-cracks of concrete.

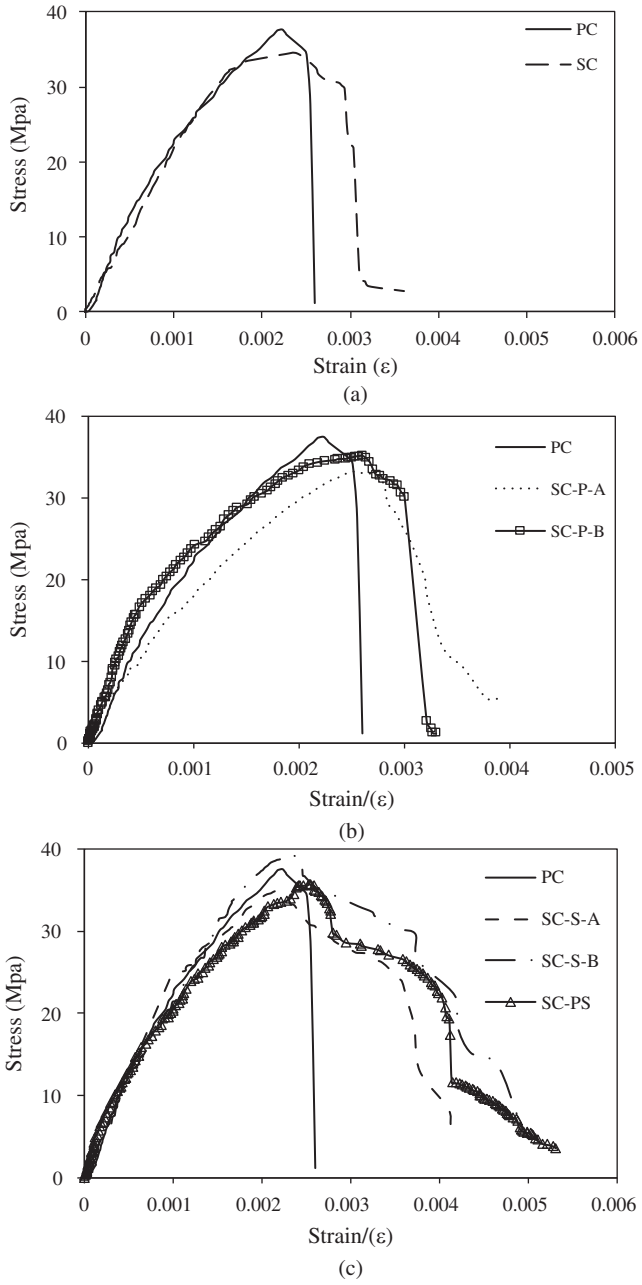

Figure 8: The stress-strain curve of specimen (a) Specimen without fibers (b) A comparison between PC and the specimens with PF (c) A comparison between PC and the specimens with SSF

Furthermore, the curve curvature of SWSSCC with SSF was lower than that of SWSSCC with PF (Figs. 8b and 8c). This indicated that the plastic deformation and micro-cracks of SC-P (SC-P-A and SC-P-B) were large compared to SC-S (SC-S-A and SC-S-B). The curve curvature increased with a decrease in polypropylene fibers content.

3. Declining Stage

The axial stress of SC and PC dropped suddenly and specimens failed quickly after the peak stress (Fig. 8a). This is because the interlocking mechanism between cement mortar and coral coarse aggregates

failed, and the main cracks quickly cross cement mortar and coral coarse aggregates. However, axial stress of SWSSCC containing SSF decreased gradually and the deformation of specimen was obvious compared to SC (Figs. 8b and 8c). It can be attributed to steel fibers not only delay the crack development but also provide an interlocking action. Furthermore, the ductility of SWSSCC was slightly improved by adding PF, which was due to the crack resistance of PF (Figs. 8b and 8c).

4 DIC Results and Discussions

An experimental campaign was developed involving uniaxial compression tests and the use of DIC method to analyze the strain distribution and crack propagation of modified SWSSCC. The DIC method can obtain surface deformation of specimen by non-destructive technique (optical technique) [31]. It assumes that the light intensity field remains point-wise unchanged. It captures the initial non-deformed image and subsequently deformed image by camera, tracks random speckle patterns in the specimen surface, and calculates cross-correlation coefficient by using the fundamental photogrammetry and digital image processing rules [32]. The displacement of speckle patterns is smoothed, and the strain of specimen is calculated by using related algorithm. Finally, the characteristics of crack are detected based on the digital image processing rules. Details of DIC program were presented in Huang et al. [33], and Matlab software was adopted to code related numerical procedure. Typical illustrations of sliced specimens are shown in Fig. 9. The obtained results provided deeper insight into the elastic development, cracking and failure of modified SWSSCC.

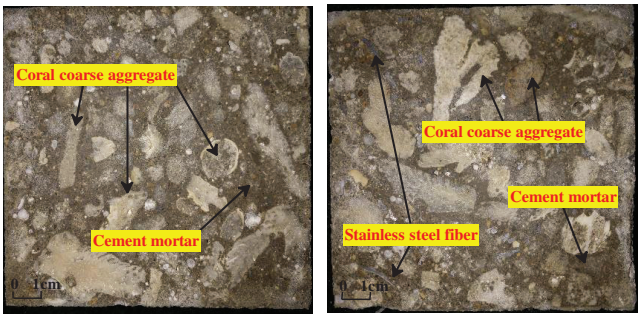

(a) (b)

Figure 9: The typical sliced specimen (a) SC (b) SC-S-B

A comparison between the calculated axial strains (through DIC method) and the real ones was performed. The differences between the test results and the results obtained by DIC method were acceptable. The mean value and standard deviation of errors were 0.089 pixel and 0.038 pixel, respectively.

4.1 The Strain Distribution

4.1.1 Axial Strain

Typical axial strain distribution of SC, SC-S-A, SC-P-B and SC-PS at different loading stages is shown in Figs. 11–13 (Fig. 10 presents the tested specimens). Axial strain distributed un-uniformly at the initial stage of loading ($0.1\sigma_{max}$) (Fig. 11), which was caused by the inhomogeneous concrete phases (cement mortar and coarse aggregates, etc.). It was found that the value of axial strain increased with the increase in stress. The high-value strain crossed the cement mortar, ITZs and coral coarse aggregates when stress reached the peak point (σ_{max}) (Fig. 12). The size of axial high-value strain increased rapidly after σ_{max} (Fig. 13). Axial strain distribution changed with the variation of stress due to the appearance of macro-cracks.

Test results indicated that the strain distribution of modified SWSSCC varied with the variation of fibers type. The differences between strain distribution of SC and that of SC-S-B, SC-P-B and SC-PS were

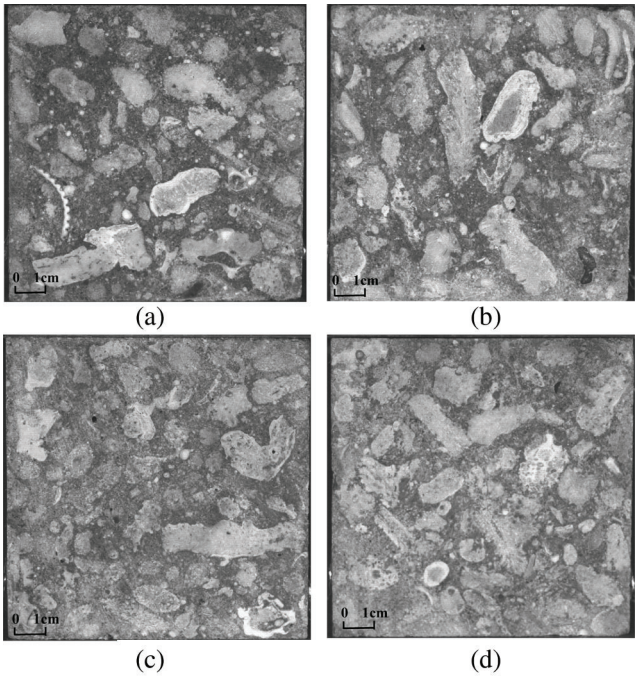

Figure 10: The tested sliced specimen (a) SC (b) SC-S-B (c) SC-P-B (d) SC-PS

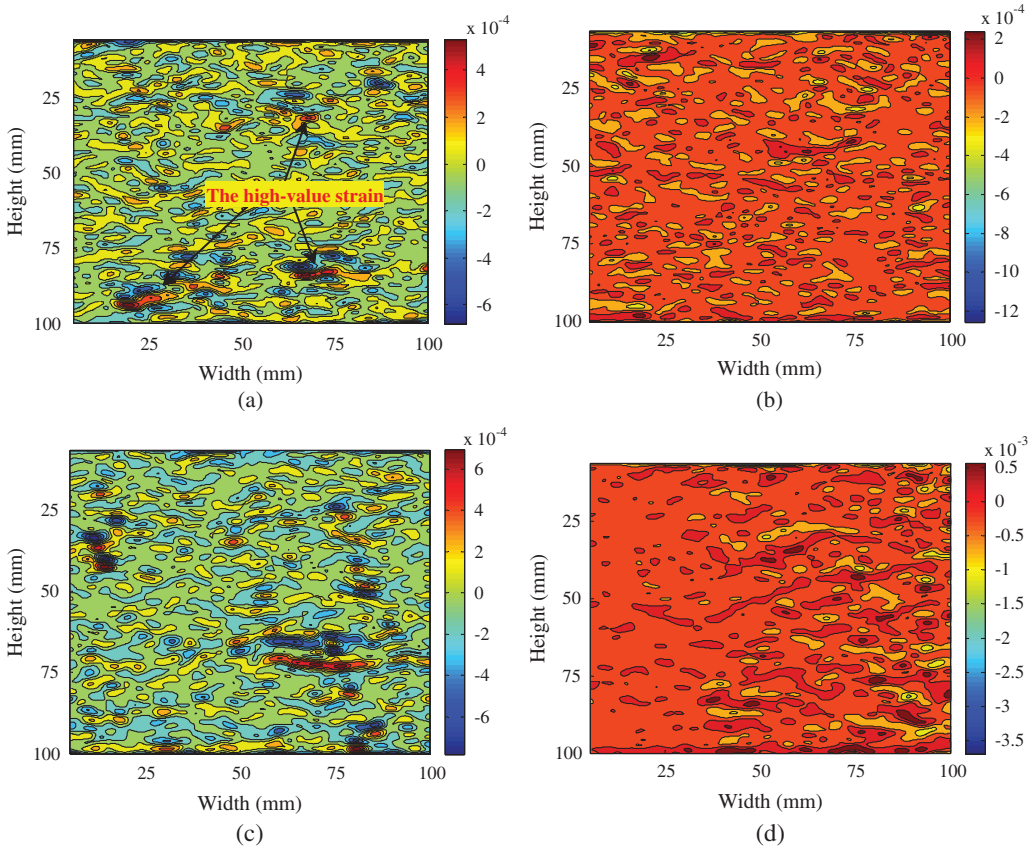

Figure 11: The distribution of axial strain at $0.1\sigma_{max}$ (unit: ε) (a) SC (b) SC-S-B (c) SC-P-B (d) SC-PS

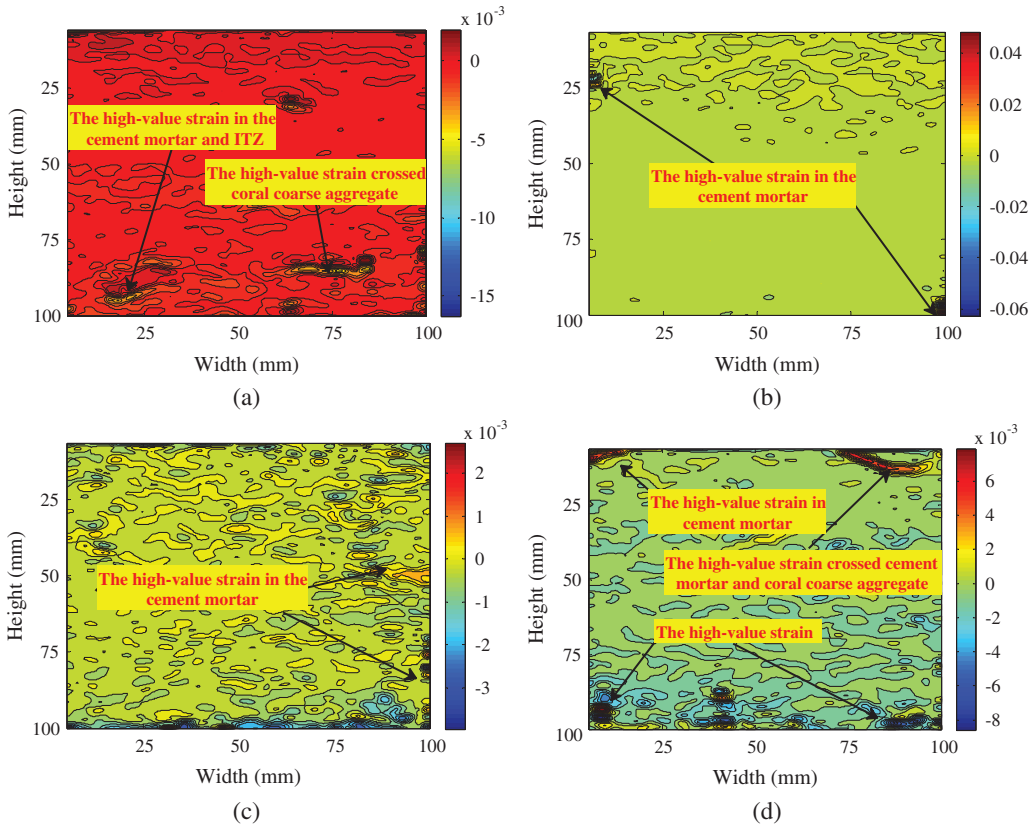

Figure 12: The distribution of axial strain at σ_{max} (unit: ε) (a) SC (b) SC-S-B (c) SC-P-B (d) SC-PS

negligible at the early stage of loading ($0.1\sigma_{max}$) (Fig. 11). However, these differences became large when axial stress approached σ_{max}. It was found that the size of axial high-value strain in SC was large compared to SC containing SSF (SC-S-B and SC-PS) (Figs. 12a, 12b and 12d). This is because the developments of cracks and plastic deformation are restricted. The high modulus and strength of SSF and the interlocking action between cement mortar and SSF hindered the crack propagation. But the differences between the axial high-value strain in SC and that in SC-P-B were small when axial stress reached σ_{max} (Figs. 12a and 12c). It can be attributed to the low modulus of PF.

After σ_{max}, the axial high-value strain distribution of SC was similar to that of SC-P-B (Figs. 13a–13d). This indicated that the influence of polypropylene fibers on deformation was negligible after the peak point.

4.1.2 Transverse Strain

Typical transverse strain distribution of specimens is shown in Figs. 14–16. It distributed irregularly (Fig. 14) at the initial stage of loading (0.1 σ_{max}), which was caused by the non-homogeneous concrete phases. Transverse strain changed with the increasing axial stress. The transverse high-value strain of modified SWSSCC crossed the cement mortar, coral coarse aggregate and ITZs when axial stress reached σ_{max} (Fig. 15). Furthermore, it was found that the transverse strain drastically increased after the peak point (Fig. 16). It is attributed to the interlocking action between CCA and cement mortar failed and the coarse aggregates are fractured.

Typical influence of fibers (PF and SSF) on the transverse strain distribution was negligible at the beginning of loading process (Fig. 14). However, the number and size of transverse high-value strains in SC-S-B and SC-PS were lower than those of transverse high-value strain in SC when axial stress

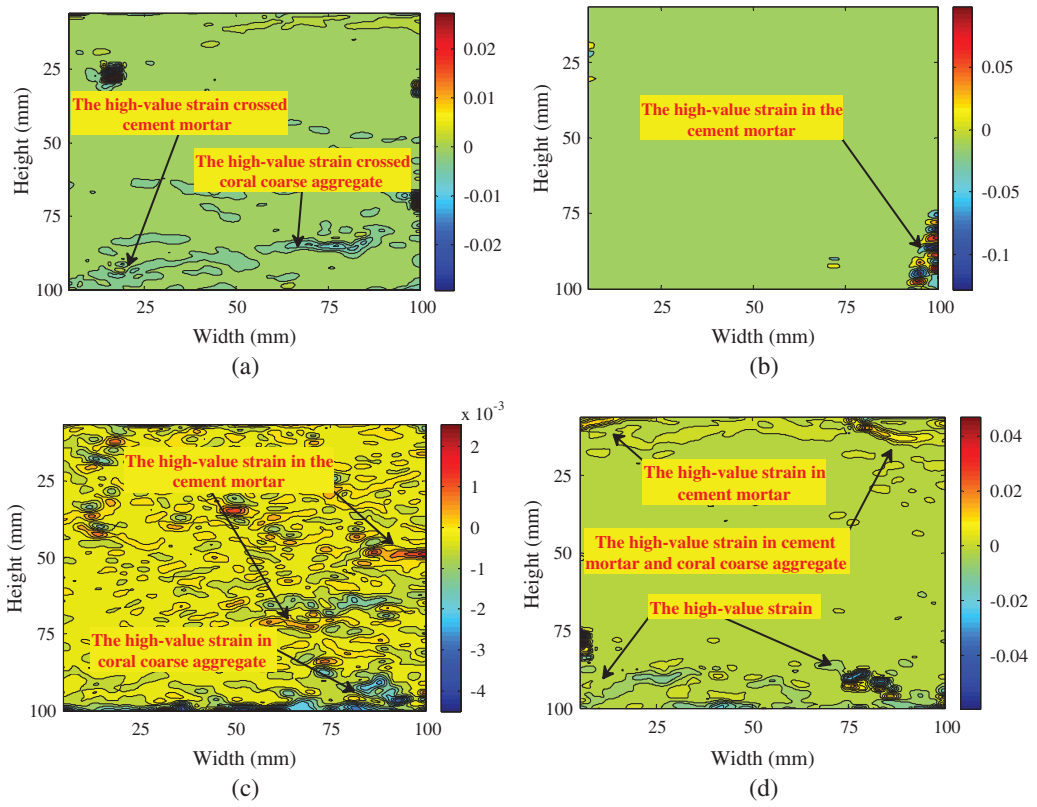

Figure 13: The distribution of axial strain at 0.9 σ_{max} (post peak point; unit: ε) (a) SC (b) SC-S-B (c) SC-P-B (d) SC-PS

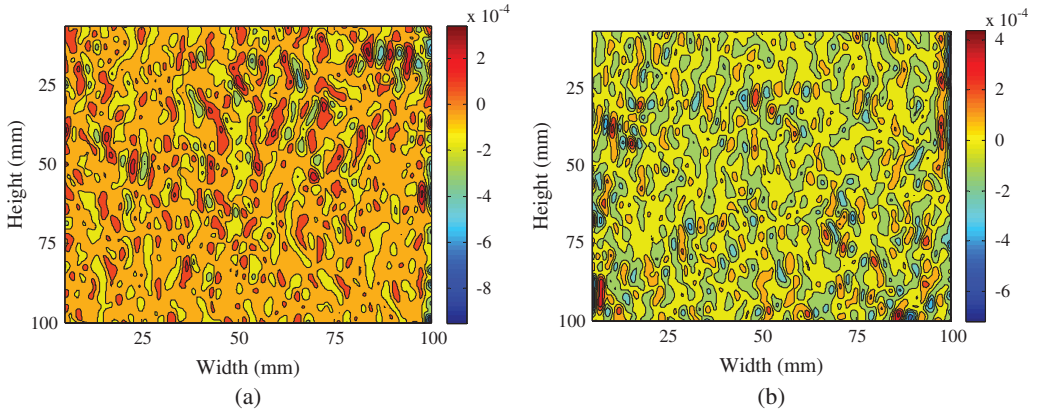

Figure 14: The distribution of transverse strain at 0.1σ_{max} (unit: ε) (a) SC-S-2 (b) SC-P-2

approached σ_{max} (Figs. 15a, 15b, 15d). The range of high-value strains in SWSSCC adopting SSF was small compared to SC-P. That can be attributed to steel fibers hinder the crack propagation of concrete effectively. Furthermore, the distribution of transverse high-value strain in SC was seldom affected by PF (Figs. 15a and 15c).

After the peak point, the transverse stain development of SC-S-B and SC-PS was slow compared to SC (Figs. 16a, 16b, 16d). Typical effect of PF on the size of transverse high-value strain (length and area) was

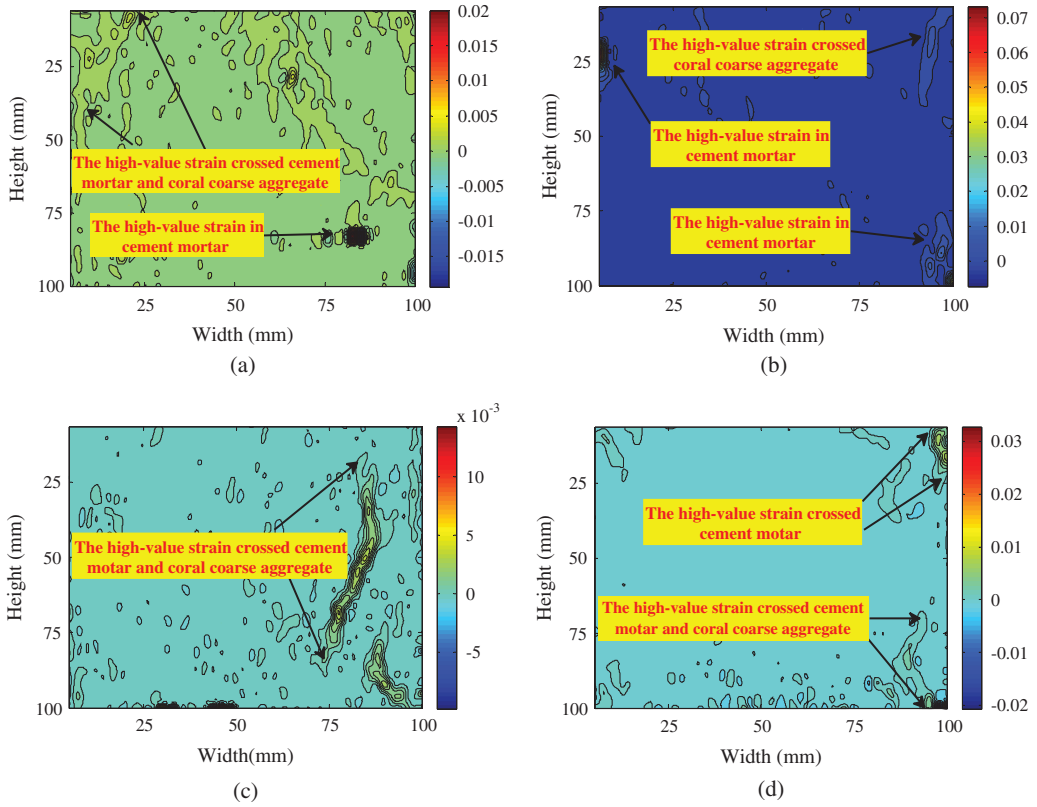

Figure 15: The distribution of transverse strain at σ_{max} (unit: ε) (a) SC (b) SC-S-B (c) SC-P-B (d) SC-PS

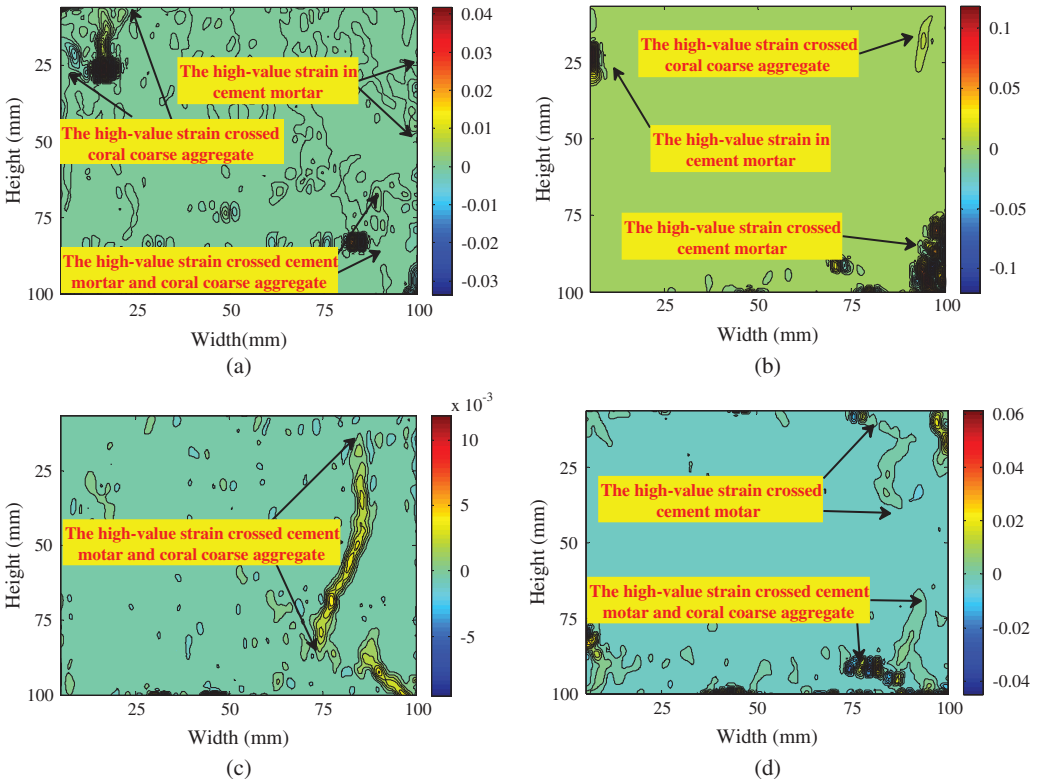

Figure 16: The distribution of transverse strain at 0.9 σ_{max} (post peak point) (unit: ε) (a) SC (b) SC-S-B (c) SC-P-B (d) SC-PS

negligible, while the value of high-value strain in SC-P-B was small compared to SC (Figs. 16a, 16c). It is attributed to the crack resistance behavior of PF.

4.2 The Characteristics of Crack Propagation

Typical crack propagation of modified SWSSCC at different loading stages is shown in Figs. 17–19. It should be noted that the map covers the entire area of the specimen photo.

It was shown that the crack development of SC was different from that of SC-PS and SC-S-B. The crack propagation of SWSSCC was hindered by SSF. The number and size of micro-cracks in SWSSCC adopting SSF (SC-S-B) were small compared to SC (Figs. 17 and 18a and 18b). The micro-cracks of SC-S-B mainly appeared in cement mortar (Figs. 18a and 18b), while those of SC appeared in coral coarse aggregates (Figs. 17a and 17b). The cracking of SC drastically increased after the peak stress compared to SC-S-B, and it crossed the cement mortar, ITZs and coral coarse aggregates of SC (Figs. 17c–17d). However, the propagation of cracks was hindered by SSF after σ_{max} (Figs. 18c–18d). Test results indicated that the number and length of cracks in SC-S-B were small (Figs. 18c–18d), while the width of main cracks was large. That is because the influence of SSF.

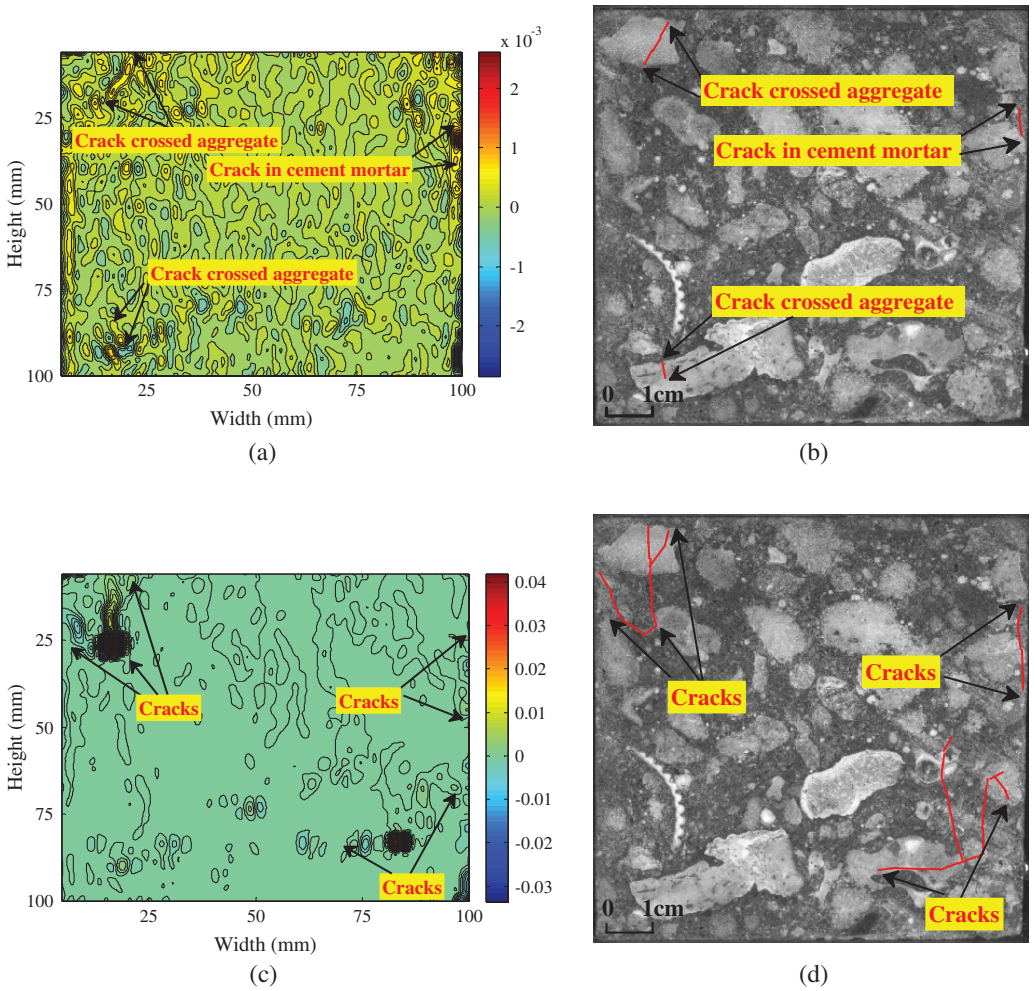

Figure 17: The crack development of SC (a) the transverse strain at 0.9 σ_{max} (b) the specimen (c) the transverse strain at 0.9 σ_{max} (post peak point) (d) the specimen

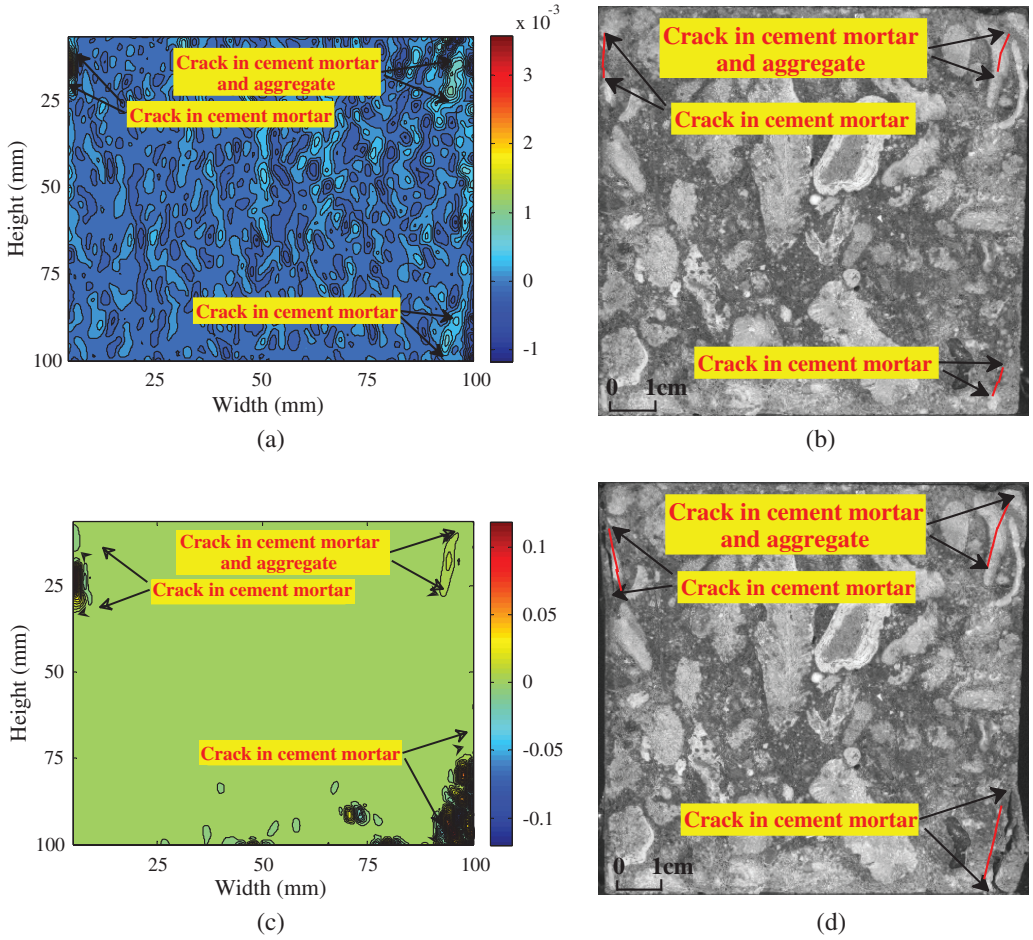

Figure 18: The crack development of SC-S-2 (a) the transverse strain at 0.9 σ_{max} (b) the specimen (c) the transverse strain at 0.9 σ_{max} (post peak point) (d) the specimen

It was found that the influence of PF on SWSSCC crack propagation was small compared to SSF. Test results indicated that the length and number of cracks in SC-P-B were higher than those of cracks in SC-S-B before σ_{max} (Figs. 18 and 19a and 19b). The micro-cracking of SC-P-B mainly appeared in cement mortar. However, the crack propagation of SC-P-B was changed after σ_{max}. It was shown that macro-cracks quickly crossed the whole surface of SC-P-B, which was different from SC-S-B (Figs. 19c–19d). Typical characteristics of SC-P-B cracks (length and numbers, etc.) after the peak point were similar to those of SC cracks (Figs. 17c and 19c). But the width of SC-P-B cracks was lower than that of SC cracks. It can be attributed to the crack resistance properties of PF.

5 Approximation of the Stress–Strain Relations

The stainless steel fibers and polypropylene fibers obviously improved the mechanical properties of SWSSCC based on the above studies. However, there were few analytical expressions for the stress-strain relation of SWSSCC adopting SSF and PF. According to experimental data and related results [2,34–36], a new expression for modified SWSSCC was suggested. The effects of fibers and composition materials (coral coarse aggregates, Cl^- and shell contents in sea water and sea sand, etc.) were considered [2,35–37]. A specific analytical stress-strain relation can be expressed as

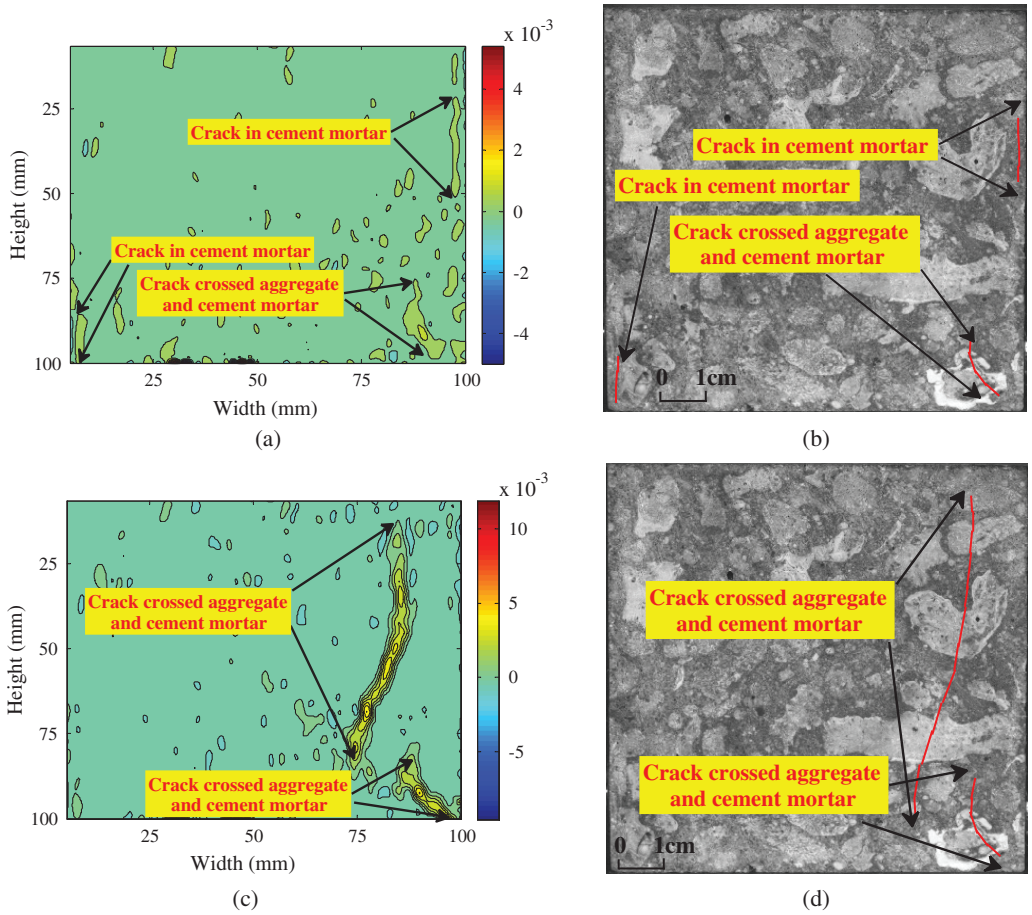

Figure 19: The crack development of SC-P-2 (a) the transverse strain at 0.9 σ_{max} (b) the specimen (c) the transverse strain at 0.9 σ_{max} (post peak point) (d) the specimen

$$y = \begin{cases} ax + (3-2a)x^2 + (a-2x^3) & 0 \le x \le 1 \\ \dfrac{x}{b(x-1)^2 + x} & x \ge 1 \end{cases} \quad (1,2)$$

In Eqs. (1–2), $y = \sigma_c/f_c$, $x = \varepsilon/\varepsilon_c$. a and b are calculated as follows. f_c and ε_c are the prismatic compressive strength and peak strain of concrete, respectively. σ_c and ε are the axial stress and strain of concrete, respectively.

Parameter a

The parameter a is the initial slope of stress-strain curve, which represents the initial modulus of specimen. The larger a is, the larger the curvature of curve is.

$$a = 1.66 - 1.74\alpha^{0.24} - 1.29\beta + 0.86\lambda_{sf} + 0.39\lambda_{pf} \quad (3)$$

In Eq. (3), α is the Cl^- content in cement mortar [37], β denotes shell content in sea sand. λ_{sf} ($\lambda_{sf} = \rho_{sf}l_{sf}/d_{sf}$) and λ_{pf} ($\lambda_{pf} = \rho_{pf}l_{sf}/d_{pf}$) represent the characteristic values of SSF and PF, respectively (Tab. 4). ρ_{sf} and ρ_{pf} are the volume fractions of SSF and PF, respectively. l_{sf} (l_{sf}) and l_{pf} (l_{pf}) represent the lengths (diameters) of SSF and PF, respectively.

Parameter b

b denotes the area under the declining part of stress-strain curve. The higher b is the less ductility of concrete is. A specific expression of b is obtained according to the test results.

$$b = 9.04 + 149.31\alpha^{0.35} - 61.06\beta - 37.47\lambda_{sf} - 9.69\lambda_{pf}. \quad (4)$$

In Eq. (4), α and β are Cl^- and shell contents, respectively. λ_{sf} and λ_{pf} are the characteristic values of SSF and PF, respectively.

A comparison between experimental curves and calculated ones are shown in Fig. 20. It was found that the difference was small. The suggested stress-strain relation can be used in theoretical analysis and practical design. Furthermore, the analytical model is applicable to modified SWSSCC with a strength grade of C30-C40, an SSF addition of 1–1.5% and a PF content of 1.0–1.5 kg/m^3.

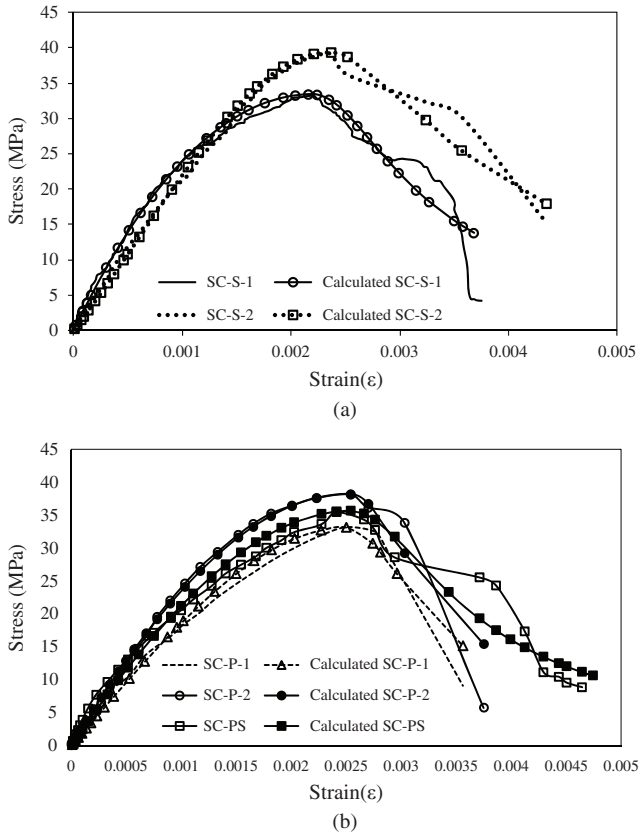

Figure 20: The comparison between the test curves and the calculated ones (a) SC-S series (b) SC-P and SC-PS series

6 Conclusions

A new experimental campaign was developed to study the mechanical properties of modified SWSSCC. The results lead to the following conclusions.

Typical failure of SWSSCC containing SSF is ductile, while the failure of SWSSCC adopting PF is brittle due to the low modulus of PF. This means that SSF effectively delay the crack propagation after the peak stress. The ductility of SWSSCC adopting SSF is acceptable.

The elastic modulus and compressive strength of modified SWSSCC increase with an increase in SSF content. However, PF obviously improves the peak strain of SWSSCC. This implies that the high modulus and strength steel fibers enhance the strength and stiffness of SWSSCC. However, low modulus PF just increases the peak deformation of SWSSCC. The strength and peak strain of SWSSCC are enhanced by adding SSF and PF simultaneously. The elastic modulus and strength of SWSSCC adopting OPC is about 5–10% higher than those of SWSSCC using LAS. This implies that high Cl^- concentration seawater decreases the sulfates attack on concrete.

The macro-cracks and high-value strain quickly cross CCA and cement mortar. The characteristics of cracks in SWSSCC containing PF are similar to those of cracks in SWSSCC. However, cracks propagation of SWSSCC adopting SSF is hindered. It implies that the development of cracks and plastic deformation is improved by SSF compared to PF.

Stainless steel fibers improve the declining stage of stress-strain curve, however, the influence of PF is negligible. This is attributed to steel fibers provide interlocking action and restrain the propagation of cracks. An analytical expression for stress-strain curve considering the influences of SSF and PF is also suggested. It characterizes the mechanical properties of modified SWSSCC. The analytical expression can be directly used in theoretical analysis and practical design, which provides a basis for the application of SWSSCC.

This study provides deeper insight into the strength, ductility, elastic development, cracking and failure of modified SWSSCC. The obtained results are necessary for the establishment of constitutive models (damage mechanics model and plasticity model, etc.). Furthermore, further studies will focus on the long-term properties of modified SWSSCC. This is because there are many chloride ions (Cl^-), sulfates (SO_4^{2-}) and shell particles in materials. The long-term properties of modified SWSSCC are complicated.

Funding Statement: This work was supported by the National Natural Science Foundation of China (Nos. 51408346, 51978389), the China Postdoctoral Science Foundation Funded Project (No. 2015M572584, No. 2016T0914), the Shandong Provincial Natural Science Foundation (No. ZR2019PEE044), the Opening Foundation of Shandong Key Laboratory of Civil Engineering Disaster Prevention and Mitigation (CDPM2019KF12), the Systematic Project of Guangxi Key Laboratory of Disaster Prevention and Structural Safety (2019ZDK035), and the Shandong University of Science and Technology (SDKDYC190358).

Conflict of Interest: The authors declare that there is no conflict of interests regarding the publication of this paper.

References

1. Da, B., Yu, H. F., Ma, H. Y., Tan, Y. S., Mi, R. Y. et al. (2016). Chloride diffusion study of coral concrete in a marine environment. *Construction and Building Materials, 123,* 47–58. DOI 10.1016/j.conbuildmat.2016.06.135.
2. Da, B., Yu, H. F., Ma, H. Y., Tan, Y. S., Mi, R. Y. et al. (2016). Experimental investigation of whole stress-strain curves of coral concrete. *Construction and Building Materials, 122,* 81–89. DOI 10.1016/j.conbuildmat.2016.06.064.
3. Yu, H. F., Da, B., Ma, H. Y., Zhu, H. W., Yu, Q. et al. (2017). Durability of concrete structures in tropical atoll environment. *Ocean Engineering, 135,* 1–10. DOI 10.1016/j.oceaneng.2017.02.020.
4. Kaushik, S. K., Islam, S. (1995). Suitability of sea water for mixing structural concrete exposed to a marine environment. *Cement and Concrete Composites, 17(3),* 177–185. DOI 10.1016/0958-9465(95)00015-5.
5. Etxeberria, M., Fernandez, J. M., Limeira, J. (2016). Secondary aggregates and seawater employment for sustainable concrete dyke blocks production: Case study. *Construction and Building Materials, 113,* 586–595. DOI 10.1016/j.conbuildmat.2016.03.097.
6. De Weerdt, K., Justnes, H. (2015). The effect of sea water on the phase assemblage of hydrated cement paste. *Cement and Concrete Composites, 55,* 215–222. DOI 10.1016/j.cemconcomp.2014.09.006.

7. Li, Q., Geng, H., Huang, Y., Shui, Z. G. (2015). Chloride resistance of concrete with metakaolin addition and seawater mixing: A comparative study. *Construction and Building Materials, 101,* 184–192. DOI 10.1016/j.conbuildmat.2015.10.076.
8. Li, Q., Geng, H. M., Shui, Z. H., Huang, Y. (2015). Effect of metakaolin addition and seawater mixing on the properties and hydration of concrete. *Applied Clay Science, 115,* 51–60. DOI 10.1016/j.clay.2015.06.043.
9. Etxeberria, M., Gonzalez-Corominas, A., Pardo, P. (2016). Influence of seawater and blast furnace cement employment on recycled aggregate concretes' properties. *Construction and Building Materials, 115,* 496–505. DOI 10.1016/j.conbuildmat.2016.04.064.
10. Mori, Y. (1981). 10 years exposure test of concrete mixed with seawater under marine environment. *Journal of Cement Association, 35,* 341–344.
11. Nishida, T., Otsuki, N., Ohara, H., Garba-Say, Z. M., Nagata, T. (2015). Some considerations for applicability of seawater as mixing water in concrete. *Journal of Materials in Civil Engineering, 27(7),* B4014004. DOI 10.1061/(ASCE)MT.1943-5533.0001006.
12. Otsuki, N., Furuya, D., Saito, T., Tadokoro, Y. (2011). Possibility of sea water as mixing water in concrete, *Conference on Our World in Concrete & Structures, Japan: Tokyo Institute of Technology.*
13. Nippon, S. A. (2012). Utilization of blast furnace slag in cement. *Nippon Slag Association, Tokyo, Japan, (In Japanese).*
14. Shi, Z., Shui, Z. H., Li, Q., Geng, H. N. (2015). Combined effect of metakaolin and sea water on performance and microstructures of concrete. *Construction and Building Materials, 74,* 57–64. DOI 10.1016/j.conbuildmat.2014.10.023.
15. Dias, W. P. S., Seneviratne, G. A. P. S. N., Nanayakkara, S. M. A. (2008). Offshore sand for reinforced concrete. *Construction and Building Materials, 22(7),* 1377–1384. DOI 10.1016/j.conbuildmat.2007.04.006.
16. Limeira, J., Agulló, L., Etxeberria, M. (2012). Dredged marine sand as a new source for construction materials. *Materiales de Construcción, 62(305),* 7–24. DOI 10.3989/mc.2011.61710.
17. Zhang, G. L., Chen, J. B., Mo, L. W., Liu, J. Z., He, Z. M. (2012). Research on influence of fly ash on the microstructural characteristics of sea sand concrete. *Applied Mechanics and Materials, 204,* 3831–3834. DOI 10.4028/www.scientific.net/AMM.204-208.3831.
18. Arumugam, R. A., Ramamurthy, K. (1996). Study of compressive strength characteristics of coral aggregate concrete. *Magazine of Concrete Research, 48(176),* 141–148. DOI 10.1680/macr.1996.48.176.141.
19. Wang, Y. G. (1988). The Feasibility of coral concrete application in the port industry. *Port & Waterway Engineering, 9,* 46–48, (In Chinese).
20. Ehlert, R. A. (1991). Coral concrete at bikini atoll. *Concrete International, 13(1),* 19–24.
21. Dempsey, J. G. (1951). Coral and salt water as concrete materials. *Journal Proceedings, 48(10),* 157–166.
22. Yang, H. C., Xiong, J. B., Wang, S. N. (2016). Effect analysis of water-cement ratio on compressive strength for coral aggregate concrete. *Construction Technology, 45(23),* 101–104 (In Chinese).
23. Huang, Y. J., He, X. J., Sun, H. S., Sun, Y. D., Wang, Q. (2018). Effects of coral, recycled and natural coarse aggregates on the mechanical properties of concrete. *Construction and Building Materials, 192,* 330–347. DOI 10.1016/j.conbuildmat.2018.10.111.
24. Wang, J., Feng, P., Hao, T. Y., Yue, Q. G. (2017). Axial compressive behavior of seawater coral aggregate concrete-filled FRP tubes. *Construction and Building Materials, 147,* 272–285. DOI 10.1016/j.conbuildmat.2017.04.169.
25. Cai, G. C., Zhao, J. (2016). Application of sulphoaluminate cement to repair deteriorated concrete members in chloride ion rich environment-A basic experimental investigation of durability properties. *KSCE Journal of Civil Engineering, 20(7),* 2832–2841. DOI 10.1007/s12205-016-0130-4.
26. Ministry of Communications of the Peoples Republic of China (2002). Standard for test method of mechanical properties on ordinary Concrete. Beijing, China, GB/T 50081-2002 (In Chinese).
27. Mehta, P. K. (1991). *Concrete in the marine environment*. London, UK: Elsevier Applied Science.

28. Ragab, A. M., Elgammal, M. A., Hodhod, O. A., Ahmed, T. E. (2016). Evaluation of field concrete deterioration under real conditions of seawater attack. *Construction and Building Materials, 119,* 130–144. DOI 10.1016/j.conbuildmat.2016.05.014.
29. Japan, C. I. (2015). *JCI technical committee report on the use of seawater in concrete*. Japan Concrete Institute, Japan.
30. Xiao, J. Z., Li, J. B., Zhang, C. (2005). Mechanical properties of recycled aggregate concrete under uniaxial loading. *Cement and Concrete Research, 35(6),* 1187–1194. DOI 10.1016/j.cemconres.2004.09.020.
31. Bolhassani, M., Hamid, A. A., Rajaram, S., Vanniamparambil, P. A., Bartoli, I. et al. (2017). Failure analysis and damage detection of partially grouted masonry walls by enhancing deformation measurement using DIC. *Engineering Structures, 134,* 262–275. DOI 10.1016/j.engstruct.2016.12.019.
32. Sutton, M. A., Orteu, J. J., Schreier, H. (2009). *Image correlation for shape, motion and deformation measurements: basic concepts, theory and applications*. Boston, USA: Springer Science & Business Media.
33. Huang, Y. J., He, X. J., Wang, Q., Xiao, J. Z. (2019). Deformation field and crack analyses of concrete using digital image correlation method. *Frontiers of Structural and Civil Engineering, 13(5),* 1183–1199. DOI 10.1007/s11709-019-0545-3.
34. Sahmaran, M., Yaman, I. O. (2007). Hybrid fiber reinforced self-compacting concrete with a high-volume coarse fly ash. *Construction and Building Materials, 21(1),* 150–156. DOI 10.1016/j.conbuildmat.2005.06.032.
35. Song, P. S., Hwang, S. (2004). Mechanical properties of high-strength steel fiber-reinforced concrete. *Construction and Building Materials, 18(9),* 669–673. DOI 10.1016/j.conbuildmat.2004.04.027.
36. Iqbal, S., Ali, A., Holschemacher, K., Bier, T. A. (2015). Mechanical properties of steel fiber reinforced high strength lightweight self-compacting concrete (SHLSCC). *Construction and Building Materials, 98,* 325–333. DOI 10.1016/j.conbuildmat.2015.08.112.
37. AASHTO (2011). *Standard method of test for sampling and testing for sampling and testing for chloride ion in concrete*. Washington, DC: American Association of State Highway and Transportation Officials.